From *ab initio* quantum chemistry to molecular dynamics: The delicate case of hydrogen bonding in ammonia

A. Daniel Boese[a)]
Department of Organic Chemistry, Weizmann Institute of Science, 76100 Reḥovot, Israel

Amalendu Chandra[b)]
Lehrstuhl für Theoretische Chemie, Ruhr-Universität Bochum, 44780 Bochum, Germany

Jan M. L. Martin
Department of Organic Chemistry, Weizmann Institute of Science, 76100 Reḥovot, Israel

Dominik Marx
Lehrstuhl für Theoretische Chemie, Ruhr-Universität Bochum, 44780 Bochum, Germany

The ammonia dimer $(NH_3)_2$ has been investigated using high-level *ab initio* quantum chemistry methods and density functional theory. The structure and energetics of important isomers are obtained to unprecedented accuracy without resorting to experiment. The global minimum of eclipsed C_s symmetry is characterized by a significantly bent hydrogen bond which deviates from linearity by as much as $\approx 20°$. In addition, the so-called cyclic C_{2h} structure, resulting from further bending which leads to two equivalent "hydrogen bonding contacts," is extremely close in energy on an overall flat potential energy surface. It is demonstrated that none of the currently available [generalized gradient approximation (GGA), meta-GGA, and hybrid] density functionals satisfactorily describe the structure and relative energies of this nonlinear hydrogen bond. We present a novel density functional, HCTH/407+, which is designed to describe this sort of hydrogen bond quantitatively on the level of the dimer, contrary to, e.g., the widely used BLYP functional. This improved generalized gradient approximation functional is employed in Car–Parrinello *ab initio* molecular dynamics simulations of liquid ammonia to judge its performance in describing the associated liquid. Both the HCTH407+ and BLYP functionals describe the properties of the liquid well as judged by analysis of radial distribution functions, hydrogen bonding structure and dynamics, translational diffusion, and orientational relaxation processes. It is demonstrated that the solvation shell of the ammonia molecule in the liquid phase is dominated by steric packing effects and not so much by directional hydrogen bonding interactions. In addition, the propensity of ammonia molecules to form bifurcated and multifurcated hydrogen bonds in the liquid phase is found to be negligibly small. © *2003 American Institute of Physics.* [DOI: 10.1063/1.1599338]

I. INTRODUCTION AND MOTIVATION

Wave-function-based quantum chemistry methods as well as density functional theory (DFT) are now well established electronic structure techniques within theoretical chemistry.[1] The former is traditionally used to investigate small finite systems, i.e., "gas phase problems," whereas the latter had its first successes in solid state physics, i.e., in the framework of "periodic lattice problems." There is also ample evidence that wave-function-based quantum chemistry methods are able to predict properties of molecular systems up to virtually any desired accuracy as a result of systematically improving the correlation treatment together with the wave function representation. However, the numerical complexity, as, e.g., measured by the computer time needed for such studies, *in praxi* easily explodes either before reaching a sufficient level of accuracy or before treating systems that

are sufficiently large. DFT methods, on the other hand, are known to lead to astonishingly good predictions for a wide variety of systems at moderate cost—of course dramatic failures are also well documented in the literature. When describing molecular solids, associated liquids, or large biosystems, noncovalent interactions such as hydrogen bonds and van der Waals interactions might play an important role. The ideal approach would be to use post-Hartree–Fock methods converged to the basis set limit, which turns out to be computationally prohibitive, especially when used in conjunction with molecular dynamics. While simple DFT methods are unable to correctly describe van der Waals interactions,[2–4] hydrogen bonds are known to be well within the capabilities of DFT approaches once suitable gradient-corrected functionals are devised. A pioneering step in the early 1990s was the investigation of hydrogen bonds in the water dimer[5–7] and in small water clusters[8] based on such functionals, which are of the generalized gradient approximation (GGA) type. Soon thereafter it was demonstrated that also the structure and dynamics of *liquid bulk* water can be described faithfully.[7] Now there is ample evidence that various proper-

[a)]Electronic mail: daniel.boese@weizmann.ac.il
[b)]On sabbatical leave from: Department of Chemistry, Indian Institute of Technology, Kanpur, India 208016.

(a)   linear eclipsed

(b)   linear staggered

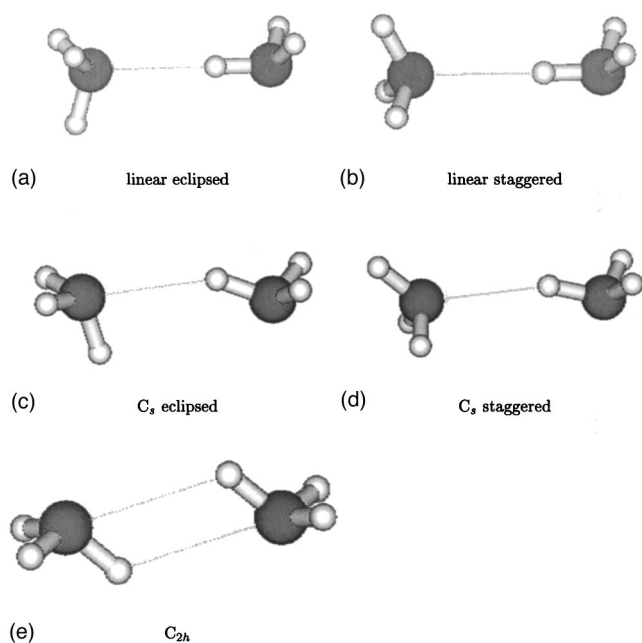(c) C_s eclipsed

(d) C_s staggered

(e) C_{2h}

FIG. 1. The five relevant optimized structures of the ammonia dimer; dotted lines are only guides for the eye.

ties of water can be computed quite reliably using GGA-type functionals, see, e.g., Refs. 7, 9–20 and Refs. 21–24 for dimer calculations. But how about other hydrogen bonded systems?

Among hydrogen-bonded dimers the ammonia dimer is peculiar since it features a rather unusual hydrogen bond, see Refs. 25 and 26 for an early and a very recent overview. Instead of an essentially linear hydrogen bond, similar to the one of the water dimer having a H–O···O angle of only 5.5°,[27] the hydrogen bond in the ammonia dimer is significantly bent as depicted in Fig. 1(c) or 1(d). Furthermore, close in energy is the so-called cyclic structure where an even more pronounced bending of the hydrogen bond produces two equivalent "hydrogen bonding contacts" according to Fig. 1(e). In addition, we point out that such strongly bent hydrogen bonds play an important role in many biological systems, in particular if the bending allows for more than one interaction of a donor with acceptor molecules which leads to so-called bifurcated or multifurcated hydrogen bonds.[28,29] In carbohydrates over 25% of the hydrogen bonds turn out to be multifurcated[28] and in proteins[30] about 40% and 90% of the hydrogen bonds in β-sheet and α-helix structures, respectively, are of this type. In this context the ammonia dimer could serve as a prototype system in order to investigate nonlinear hydrogen bonding on the level of a minimal model, i.e., a free dimer in the gas phase.

Guided by analogy or chemical intuition, one might guess that the ammonia dimer possesses a "classical" quasi-linear hydrogen bond similar to other dimers such as those of water or hydrogen fluoride. Early calculations, see, e.g., Refs. 31–33 and references cited therein, actually assumed from the outset a perfectly linear bond similar to the one shown in Fig. 1(a) or 1(b) or predicted a quasilinear hydrogen bond as depicted in Fig. 1(c) or 1(d), while others[34–36] favored strongly bent up to cyclic dimers similar to Figs.

1(c)–1(e). This controversy got fueled by microwave measurements[37] providing evidence for a quasirigid cyclic structure such as the one in Fig. 1(e). The issue of a quasi-linear hydrogen bond versus a cyclic structure remained controversial (see, e.g., Refs. 38 and 39) up to early 1990s where both experiment and theory started to converge. Thanks to sophisticated experiments[40–47] and extensive computations[48,49] there is now consensus[26] that the ammonia dimer is a *fluxional* molecular complex with an equilibrium structure that is characterized by a bent hydrogen bond such as the one shown in Fig. 1(c). Combining far-infrared spectra with static and dynamic calculations,[48–50] the H–N···N hydrogen bond angle (between the N–H bond of the proton donor and the N···N axis) was determined to be 26° in the equilibrium structure with a N···N distance of ≈3.354 Å. Note, however, that this "experimental" structure of the ammonia dimer was deduced within the rigid monomer approximation,[48,50] which might introduce a systematic bias. In fact, a recent study[51] of the water dimer has shown that monomer flexibility is indeed important in determining its vibration–rotation–tunneling spectrum and thus "experimental" structures derived from it. It is expected that such monomer flexibility would also be important for the ammonia dimer. Furthermore, the global potential energy surface is found to be very flat,[48,49] e.g., the cyclic C_{2h} structure was estimated to be about only 7 cm^{-1} higher in energy, which is qualitatively consistent with the observation that the dimer is a very fluxional complex. Most interestingly, there is now experimental support[52] advocating a more cyclic equilibrium structure for $(NH_3)_2$ in superfluid helium droplets at 0.4 K.

More recent wave-function-based quantum chemical calculations[53,54] on the structure and energetics of the ammonia dimer support in some aspects the earlier conclusions.[26,48,49] Second-order Møller–Plesset perturbation calculations (MP2) with medium-sized basis sets (for geometry optimization followed by fourth-order Møller–Plesset single-point energy calculations)[53] resulted however in a significantly smaller H–N···N hydrogen bond angle of 12° together with a reasonable low barrier of 7.6 cm^{-1}. Most recently, another (valence-only) MP2 study,[54] this time near the one-particle basis set limit, was reported. At the MP2 limit, the hydrogen bond angle of 23° was closer to the recommended value,[48,49] but the barrier of 24 cm^{-1} seems too high and the dissociation energy D_e (into separated and optimized monomer fragments) was estimated to be 13.5±0.3 kJ/mol. This clearly hints to the importance of higher-order correlation effects and core–valence corrections, in particular since they account for 0.4 kJ/mol in the case of the water dimer[55] (which already exceeds the error bar given in Ref. 54). DFT calculations of the ammonia dimer are both rather scarce[56–59] and somewhat inconclusive as to what level of accuracy DFT methods describe this intermolecular interaction. In the following we will clearly demonstrate that none of the 14 widely used GGA, meta-GGA, and hybrid functionals checked by us lead to a satisfactory description of both the structure and relative energies of the ammonia dimer (despite large basis sets being used and basis set superposition error being corrected for). Thus, even at the level

of the ammonia dimer there is still room for improvement based on purely theoretical grounds!

Thus far we considered the behavior of ammonia in the limit of forming a dimer, e.g., in the gas phase. The question arises, if or how its peculiar behavior concerning hydrogen bonding in the dimer is present in its condensed phases. Indeed, based on the *apparent* stability and rigidity of the *cyclic* dimer in the gas phase[37] it was concluded in quite general terms some time ago that NH_3 might well be best described as a powerful hydrogen-bond acceptor with little propensity to donate hydrogen bonds;[25] note that now it is however recognized that the ammonia dimer is nonrigid and noncyclic.[26] The x-ray structure of *crystalline* ammonia at low temperatures[60,61] features a staggered, directed hydrogen bonded network, with the monomers being arranged like the dimer in Fig. 1(d). Furthermore, based on neutron powder diffraction experiments, it was proposed that solid ammonia has an "unusual shared-hydrogen bond geometry" [62] and, in particular, the high-pressure phase $ND_3 - IV$ contains bifurcated hydrogen bonds with bending angles as large as about 30°. A most recent theoretical study,[63] however, did not support the presence of bifurcated hydrogen bonds in phase IV of solid ammonia. In this latter study, it was concluded through calculations of electron density between intermolecular nitrogen and hydrogen atoms that the apparent bifurcated hydrogen bond geometry in solid ammonia IV is actually a single hydrogen bond perturbed by a neighboring interacting atom. The structure of *liquid* ammonia has been studied by x-ray[64] and neutron[65] diffraction for a long time. Only the total structure factor and the total radial distribution function could be extracted in these early experiments and the presence of hydrogen bonds in liquid ammonia was inferred from a comparison of the experimental structure factor with the known structure of the solid. More recently, a set of neutron diffraction experiments was performed[66] on liquid NH_3, ND_3, and an iso-molar NH_3/ND_3 mixture. The powerful isotopic substitution technique, in conjunction with sophisticated data analysis, allowed extraction of all partial radial distribution functions at 213 and 273 K. Contrary to earlier conceptions (as presented in many standard textbooks on that subject) the spatial arrangement of nitrogen atoms showed that no extended hydrogen bonded network exists in liquid ammonia. Nevertheless, some degree of hydrogen bonding was inferred from the temperature dependence of the N–H and H–H radial distribution functions. However, the hydrogen bond interaction in liquid ammonia proved to be much weaker than that in water and no clear hydrogen bond peak was observed in either N–H or H–H correlations, unlike the case of water.

Due to the importance of liquid ammonia and in particular its metallic solutions, many theoretical attempts have been made in the past two decades to understand its liquid phase. Most of these studies are based on classical Monte Carlo or molecular dynamics (MD) simulations using empirical site–site[67–73] or *ab initio* pair potentials[74] which all lead to essentially linear hydrogen bonds in the limit of treating the ammonia dimer. A recent pioneering study[59] investigated the structure of liquid ammonia through Car–

Parrinello *ab initio* molecular dynamics,[75,76] i.e., without resorting to any predetermined (pairwise) potentials but using the full many-body interactions as obtained by "on the fly" DFT (using the Becke–Lee–Yang–Parr, BLYP functional) instead. It was found that the results of the N–N, N–H, and H–H radial distribution functions are in better agreement with experimental results than previous calcuations relying on model potentials. Some important differences, however, still remained. For example, the results of this study were found to overestimate the hydrogen bonded structure as revealed by the N–H correlations and predict a narrower first peak of the N–N distribution when compared with the corresponding experimental results. Also, a later such study[77] of liquid ammonia containing an ammonium or an amide solute reported somewhat different results for the N–N and N–H correlations between the bulk ammonia molecules compared to those of Ref. 59. Besides, the nature of the hydrogen bonds in the liquid phase is not fully understood yet, in particular in view of the experimental situation. As discussed before, unlike water, the ammonia dimer has a bent hydrogen bond in its equilibrium geometry. If this bent character of the dimer hydrogen bond has the same significant effects on the liquid as in solid phases[62] is still an unresolved issue, in particular since all pair potentials by construction yield a quasilinear hydrogen bond as do existing density functionals.

The outline of this paper is as follows: In Sec. II, we describe the details of the computational methodologies that we employ for the calculations of the dimer and the liquid phase. In Sec. III, we present results for important dimer structures and their energies based on highly accurate *ab initio* methods and compare these data to those obtained from a wide variety of currently available density functional families. Section IV focuses in detail on the development of the novel HCTH/407+ functional, on its performance in various systems, and on the improvement achieved on the dimer level. In Sec. V, we compare the results of *ab initio* MD simulations of liquid ammonia using HCTH/407+ to those obtained from the widely used BLYP functional for reference purposes, and to experimental data wherever available. We summarize and conclude in Sec. VI.

II. METHODS AND TECHNICAL DETAILS

A. The HCTH density functional family

In this contribution, we develop a new GGA functional—which will be termed HCTH/407+—that only involves the density $\rho(\mathbf{r})$ and its gradient $\nabla\rho(\mathbf{r})$. The latter has been shown to be a necessary ingredient for the description of hydrogen bonds within DFT, see for instance Refs. 5–8, 22, 24, and 78. Contrary to the so-called hybrid functionals that involve "Hartree–Fock exchange" (such as, e.g., B3LYP[79]), this advantage is not impaired by a prohibitive computational overhead relative to the local (spin) density approximation if used in the framework of plane wave pseudopotential calculations, see, e.g., the arguments presented in Sec. 3.3 of Ref. 76. Thus, we opted for reparametrizing the Hamprecht–Cohen–Tozer–Handy (HCTH) form, which has been described in detail elsewhere[80] and was originally used by Becke for a hybrid functional.[81] In

general, HCTH is a post-local spin density approximation (post-LSDA) functional, meaning that it factorizes the LSDA functional forms (F_{LSDA})

$$E_{xc} = \sum_{\gamma = x, c_{\sigma\sigma}, c_{\alpha\beta}} E_\gamma$$
$$= \sum_\gamma \sum_{q=0}^m c_{q,\gamma} \int F_{LSDA,\gamma}(\rho_\alpha, \rho_\beta) u_\gamma^q(x_\alpha^2, x_\beta^2) d\mathbf{r}. \quad (1)$$

Here, u_γ^q denotes the perturbation from the uniform electron gas if $c_{0,\gamma}$ is unity. The sum over the integers q going from zero to m implies the power series defined through u_γ, with $\theta_{\gamma\sigma}$ and $\eta_{\gamma\sigma}$ as fixed coefficients:

$$u_\gamma^q(x_\alpha^2, x_\beta^2) = \left(\frac{\theta_{\gamma\sigma} x_\sigma^2}{1 + \eta_{\gamma\sigma} x_\sigma^2} \right)^q. \quad (2)$$

The variable x_σ is closely related to the reduced density gradient

$$x_\sigma^2 = \frac{(\nabla \rho_\sigma)^2}{\rho_\sigma^{8/3}}. \quad (3)$$

This functional form was previously employed for reparametrizations[17,82] resulting in a highly accurate GGA functional, HCTH/407.[82] Although the above form obeys none of the exact conditions for slowly varying densities,[83] and violates part of the scaling relations,[84] it does obey the most crucial scaling relations and the Lieb–Oxford bound[85,86] within the physically important region.[87]

When employing the form in Eq. (1) up to fourth order in m, we obtain 15 linear coefficients (because of having exchange, like-spin and opposite-spin correlation), which are easily parametrized by minimizing an error function Ω, which is constructed out of the sum of three components,

$$\Omega = \sum_m^{n_E} w_m (E_m^{exact} - E_m^{KS})^2 + \sum_{l,X}^{n_G} w_{l,G} \left(\frac{\partial E_l^{KS}}{\partial X} \right)^2$$
$$+ \sum_{j,\sigma}^{n_v} w_{j,v} \int (v_{j,\sigma}^{ZMP} + k_{j,\sigma} - v_{j,\sigma}^{KS})^2 \rho_{j,\sigma}^{2/3} d\mathbf{r}. \quad (4)$$

The three sums represent the mean-square deviations from our reference data of energies, gradients, and exchange-correlation potentials for each molecule, respectively, of the result of a Kohn–Sham density functional calculation (denoted by the superscript "KS"). In the case of the total energies reference data are high-level quantum chemistry results that are denoted by "exact." In the second sum the exact gradients (at equilibrium geometry) are zero by definition and thus do not appear in the formula. In the final term, we fit to the exchange-correlation potentials as determined by the Zhao–Morrison–Parr (ZMP) method,[88] which are shifted by a constant k because of the effects of the quantum-mechanical integer discontinuity. The ZMP method has been proven to be an important aspect of the fit.[89] All these contributions need to be balanced using weights w, which have been determined and reported previously.[82] The weights w consist of a product of multiple partial weights making contributions for each molecule in order to ensure a balanced functional.

We also have to consider the molecular set for which the new functional was determined. In general, the new HCTH/407+ functional was determined by fitting it to the "407 set" of molecules as used for HCTH/407.[90] This set is similar to the G3 set of molecules,[91] with added inorganic molecules, but a smaller proportion of large organic species which we considered to be over-represented. This original training set was supplemented with data from the ammonia dimer, including nonequilibrium structures, as described in detail in Sec. IV.

B. Quantum chemical calculations

For the accurate determination of some points of the potential energy surface (PES) of the ammonia dimer, we used the W2 method.[92] This is basically an extrapolation toward the full coupled-cluster single double (triple) CCSD(T) basis set limit including relativistic (but not Born–Oppenheimer) corrections. W2 energies are calculated at the CCSD(T)/A′PVQZ geometry, this notation meaning an aug-cc-pVQZ basis set for nitrogen and a cc-pVQZ basis set for hydrogen.[93] The MOLPRO package[94] was used for these calculations. This method is one of the most accurate standard *ab initio* methods currently available, with an average error of less than 0.5 kcal/mol for the G2-1 set[95] of molecules.[96] In particular, it is more reliable and accurate than the G1, G2, and G3 methods (although computationally much more expensive).[96,97]

Two types of higher-order contributions were considered. First, higher-order T_3 effects were assessed by means of full CCSDT[98] calculations using the ACESII program system.[99] Second, the importance of connected quadruple excitations was probed by means of CCSD(TQ)[100] and BD(TQ)[101,102] calculations using ACESII and GAUSSIAN 98,[103] respectively.

For the DFT calculations, we employed the Cadpac suite of programs,[104] and assessed a variety of GGA and meta-GGA functionals (namely BLYP,[105] PBE,[106] HCTH/120,[17] HCTH/407,[82] τ-HCTH,[24] and BP86;[107] we also tested but do not report results from PW91[108] and HCTH/93[80]) and hybrids (B3LYP,[79] B97-1,[80] and τ-HCTH hybrid;[24] not reported are the results obtained from B97-2[109] and PBE0[110]). In case of the density functional calculations we used an A′PVTZ basis set, which is reasonably close to the DFT basis set limit.

For the DFT values, which were obtained from using finite basis sets without extrapolation of the W1/W2 type, we employed the counterpoise (CP) correction[111] to account for the basis set superposition error (BSSE). In the fitting procedure, the TZ2P basis set[112] was utilized in addition to the A′PVTZ basis set.

C. *Ab initio* molecular dynamics simulations

The *ab initio* molecular dynamics simulations were performed by means of the Car–Parrinello method[75,76] and the CPMD code.[76,113] A simple cubic box of 32 ammonia molecules with a box length of 11.229 Å was periodically replicated in three dimensions and the electronic structure of the extended system was represented by the Kohn–Sham

J. Chem. Phys., Vol. 119, No. 12, 22 September 2003

Hydrogen bonding in ammonia   5969

TABLE I. Dissociation energies D_e (in kJ/mol) according to Wn theories for several hydrogen bonded dimers compared to the best available estimates from Refs. 55, 117, and 118.

Molecule	W1	W2	Reference
$(HF)_2$	19.13	19.10	19.10 ± 0.2 (117)
$(H_2O)_2$	20.93	20.84	21.1 ± 0.3 (55)
$(H_2O)(NH_3)$	26.94	26.82	27.4 ± 3 (118)

TABLE II. Relative energies (in cm^{-1}) according to Wn theories for the ammonia dimer at the respective CCSD(T)/A$'$PVQZ optimized structures compared to the global minimum; for the latter the dissociation energies D_e (in kJ/mol) into isolated optimized monomers are reported in the last line. In column 2, and column 4, standard W1 and W2 results are reported, while in column 3, a counterpoise-correction is employed on each step in the W2 calculation.

Points on PES	W1 (w BSSE)	W2 (w/o BSSE)	W2 (w BSSE)	Best estimate
C_s (staggered)	23.4		23.5	23 ± 5
C_{2h}	0.7	5.9	2.8	3.5 ± 3
Linear (eclipsed)	69.6		67.5	67 ± 5
Linear (staggered)	71.8		69.9	70 ± 5
Global minimum				
C_s (eclipsed)	13.21	13.15	13.13	13.1 ± 0.2

formulation[114] of DFT within a plane wave basis. The core electrons were treated via the atomic pseudopotentials of Goedecker *et al.*[115] and the plane wave expansion of the KS orbitals was truncated at a kinetic energy of 70 Ry. A fictitious mass of $\mu = 875$ a.u. was assigned to the electronic degrees of freedom and the coupled equations of motion describing the system dynamics were integrated using a time step of 5 a.u. As is usually done, see, e.g., Refs. 7, 9, and 10, the hydrogen atoms were given the mass of deuterium in order to allow for a larger molecular dynamics time step which also reduces the influence of (the neglected) quantum effects on the dynamical properties.

The *ab initio* MD simulations have been performed using the HCTH/407+ and BLYP[105] functionals. We used the BLYP functional in addition to the new functional because the former has been shown to provide a good description of hydrogen bonded liquids such as water,[7,10,11] methanol,[116] and also ammonia.[59,77] Thus, it is worthwhile to compare the results of the two functionals for various structural and dynamical properties of liquid ammonia. The initial configuration of ammonia molecules was generated by carrying out a classical molecular dynamics simulation using the empirical multisite interaction potential of Ref. 71. Then, for simulation with the HCTH/407+ (BLYP) functional, we equilibrated the system for 8.75 (10.1) ps at 273 K in *NVT* ensemble using Nose–Hoover chain method and, thereafter, we continued the run in *NVE* ensemble for another 9.30 (9.34) ps for calculation of the various structural and dynamical quantities; the average temperatures of these microcanonical runs were about 275 (252) K. We note that the size of the simulation box used in the present simulations corresponds to the experimental density of liquid ammonia at 273 K, which is 2.26×10^{-2} molecules/ Å^3.[66]

III. THE AMMONIA DIMER: STRUCTURE AND ENERGETICS

In order to briefly validate the W2 method for some representative hydrogen bonded systems, $(HF)_2$ and $(H_2O)_2$, we compared the W2 results to MP2 basis set limit corrections applied to coupled cluster calculations,[55,117] while the reference data were additionally empirically refined by scaling the calculations to certain quantum energy levels. Moreover, to get an estimate of the accuracy of the basis set extrapolation, we compared with the more cost-effective alternative of W2, which is W1.[92] When calculated at the same geometry as W2, it usually yields a fair estimate as to how well the basis set limit is obtained in the extrapolation. In Table I, the dissociation energies for the HF and H_2O dimers are compared to best values from the literature,

and displayed along with the results for the $(NH_3)(H_2O)$ complex. All the W1 and W2 results are within the stated error margins of the reference data. While the dissociation energy of the hydrogen fluoride dimer is exactly the same, that of water dimer is slightly lower than predicted in Ref. 55. In the latter case, relativistic corrections were not included in their best estimate. This will reduce the energy somewhat; however we would expect a geometry relaxation to lower the energy. The authors of Ref. 55 used a CCSD(T)/ aug-cc-pVTZ geometry and estimated the geometry relaxation, whereas the W2 calculation is carried out at a CCSD(T)/A$'$PVQZ geometry. Nevertheless, the results show only 0.03 kJ/mol difference between the W1 and W2 methods for the HF dimer and 0.09 kJ/mol for the water dimer, indicating the high accuracy of these methods for such interactions. Finally, the $(H_2O)(NH_3)$ dissociation energy is predicted to be 26.8 kJ/mol by W2, compared to 27.4 kJ/mol determined by experiment;[118] unfortunately no high-level *ab initio* data were found in the literature for this mixed dimer.

Let us now focus on the ammonia dimer. Five different structures on the dimer PES can be considered important. The global minimum found on the CCSD(T)/A$'$PVQZ surface, as shown in Fig. 1(c), has an HNN angle of 19.9° with eclipsed hydrogens and C_s symmetry. Its staggered counterpart, displayed in Fig. 1(d), has an HNN angle of 13.1°. The two completely linear structures with the HNN angle being 0° [Figs. 1(a) and 1(b)] are salient points and the C_{2h} structure [Fig. 1(e)] is a transition state. In Table II, W1 and W2 results for the five structures are summarized, with columns two and four (with BSSE) corresponding to the regular W2 method without the CP-correction. Because of the low barrier between the C_s minimum and the C_{2h} structure, we additionally calculated a counterpoise-corrected W2 barrier. As to the accuracy of the electron correlation methods underlying the W2 method, we can make the following observations:

(1) Quasiperturbative connected triple excitations, i.e., the CCSD(T)–CCSD difference, only contribute 0.5 cm^{-1} to the C_{2h} barrier with CP correction and 0.7 cm^{-1} without.

(2) This has also been verified by CCSD(TQ) [BD(TQ)] cal-

TABLE III. Various first principles results for the dissociation energies D_e (in kJ/mol) of the eclipsed C_s global minimum and relative energies (in cm^{-1}) of several structures of the ammonia dimer with respect to the global minimum. All data, except that for W2, were obtained using an A$'$PVTZ basis set at fully optimized geometries including the counterpoise correction. W1 and our best estimates for these values are reported in Table II.

Geometry type method	C_s (ecl) D_e (kJ/mol)	C_s (sta) difference (cm^{-1})	C_{2h} difference (cm^{-1})	Lin (ecl) difference (cm^{-1})	Lin (sta) difference (cm^{-1})
W2	13.13	23.5	2.8	67.5	69.9
CCSD(T)	12.22	18.2	2.8	62.8	63.8
CCSD	11.31	18.4	3.3	60.7	59.4
MP2	12.27	20.3	2.9	71.8	72.7
HF	7.58	12.6	23.6	32.3	34.4
BLYP	9.11	5.7	97.8	36.5	36.4
PBE	13.05	9.2	91.5	42.1	41.4
HCTH/120	9.48	6.2	75.1	31.1	32.4
HCTH/407	11.23	11.0	27.0	39.0	41.1
τ-HCTH	10.96	5.2	141.8	29.9	29.6
B3LYP	10.18	3.3	76.6	40.2	40.1
B97-1	12.73	11.2	61.1	41.5	41.6
τ-HCTH hyb	11.27	9.4	99.9	37.7	37.2
HCTH407+	13.18	18.0	4.0	51.5	53.6

culations, where the contribution of the perturbative connected quadruples lowers the barrier by 0.2 cm^{-1} [0.3 cm^{-1}] with the A$'$PVDZ basis set.

(3) Higher-order connected triples [i.e., CCSDT-CCSD(T)] additionally lower the barrier by 0.2 cm^{-1} when using A$'$PVDZ. This leads to the conclusion that not only has basis set convergence been achieved, but also that higher-order excitations beyond CCSD(T) will contribute less than 1 cm^{-1}.

(4) Further optimization of the C_s geometry at the MP2/A$'$PV5Z level lowers the binding energy by only 0.3 cm^{-1} (0.004 kJ/mol) relative to MP2/A$'$PV5Z//MP2/A$'$PVQZ.

(5) We do not expect relaxation of the geometry at the core-valence level to make a significant contribution, since even for the monomer the core-valence correction to the geometry is very small.[119]

Still, the difference between the BSSE-corrected and uncorrected results is rather large. Based on these results, we suggest that the C_s to C_{2h} energy difference is 3.5 ± 3 cm^{-1}, and we would expect the barriers between the linear and minimum geometries to be equally well described by W2. For the slightly improved CCSD(T) geometry, by correcting CCSD(T)/A$'$PVQZ-MP2/A$'$PVQZ+MP2/A$'$PV5Z, we predict the HNN angle to be 20.7°. As for the C_{2h} barrier, the interaction energy is raised by 0.002 kJ/mol when going from CCSD(T) to CCSDT, showing that the quasiperturbative triples treatment (and the quadruples estimation as well) is quite accurate. Using an A$'$PVDZ basis set, the quasiperturbative quadruples treatment lowers the binding energy by 0.092 kJ/mol for the coupled cluster and 0.087 kJ/mol when using the Brueckner–Doubles method. With the geometry relaxation contributing less than 0.005 kJ/mol at MP2 level and the estimate of the higher order excitations, we predict the dissociation energy to be 13.1$\pm$0.2 kJ/mol, since the main error is likely to come from the quadruple excitations.

The results obtained using a selection of currently published functionals are shown in Table III. For comparison, the CCSD(T), CCSD, MP2, and HF values are given. It should be noted, however, that BSSE for the coupled-cluster values is more than twice as high as for DFT (0.9 compared to 0.4 kJ/mol), and therefore we would expect the DFT calculations to be closer to their respective basis set limits than the *ab initio* methods. Nevertheless, their BSSE is still larger than that at the HF level. As expected, the CCSD(T) and W2 numbers are reasonably close to each other. Most density functional methods reproduce the dissociation energy as listed in the first column, reasonably well. In general, the GGA and meta-GGA functionals tested give a good description of this interaction underestimate and PW91 overestimating the dissociation energy. The tested hybrid functionals are even more accurate, yet all of them underestimate the dissociation energy.

However, if we consider the energy difference between the staggered and eclipsed conformation of the NH$_3$ dimer (see the data in the second column of Table III), it becomes obvious that available functionals are incapable of reproducing the effect of a bent hydrogen bond. It is found that density functionals typically underestimate the difference between the local and global minima by at least a factor of 2. We note here that functionals other than those listed in our tables (such as, e.g., PW91, B97-2, PBE0) yield similar results which are therefore not displayed. On the other hand, all other wave-function-based *ab initio* methods considered are able to reproduce this effect. This becomes even more apparent when considering the C_{2h} transition state. Here, the coupled-cluster differences are close to 3 cm^{-1}, whereas HF renders 24 cm^{-1} and the DFT values are between 60 and 95 cm^{-1} with the exception of HCTH/407 (27 cm^{-1}) and the τ-HCTH functionals (100 and 140 cm^{-1}). In turn, the other barrier is underestimated by 30%–60% and both linear structures are stabilized relative to the global minimum. The same trends are seen in Table IV, where the HNN angles of

TABLE IV. Various first principles results for representative structural parameters of the ammonia dimer, see Fig. 1, using the A′PVTZ basis set.

Geometry type	C_s (ecl) N···H distance	C_{2h} N···H distance	C_s (ecl) HNN angle	C_s (sta) HNN angle
Best estimate	2.31	2.52	20.7	13.2
CCSD(T)[a]	2.302	2.522	19.86	13.09
CCSD(T)	2.294	2.527	16.40	12.43
CCSD	2.331	2.562	16.76	12.39
MP2	2.286	2.520	17.32	13.28
HF	2.541	2.772	13.41	9.69
BLYP	2.341	2.610	9.73	8.55
PBE	2.249	2.512	9.90	8.47
HCTH/120	2.427	2.736	10.27	8.65
HCTH/407	2.493	2.773	13.71	10.25
τ-HCTH	2.311	2.645	8.40	7.45
B3LYP	2.322	2.573	10.50	8.89
B97-1	2.298	2.555	10.90	9.00
τ-HCTH hyb	2.269	2.549	9.57	8.24
HCTH/407+	2.493	2.754	16.95	11.33

[a]A′PVQZ basis set.

the two minimum structures are shown. Here, available density functionals underestimate the bending of the hydrogen bond by almost a factor of 2 for the global minimum and by about 30% for the local (staggered) minimum, although the hydrogen bond distance itself is reasonably well reproduced. Both τ-HCTH functionals, while they perform well with their large ''training'' fit set, are the worst performers here. On the other hand, HCTH/407 is the only functional which is somewhat capable of reproducing the effect, outperforming Hartree–Fock.

In summary, although standard density functionals do yield a correct dissociation energy and a slightly nonlinear hydrogen bond, they completely overestimate the barrier toward the symmetrical C_{2h} structure, thereby preferring a much more linear hydrogen-bonding configuration than our accurate reference methods. Although the energy differences might be viewed as intrinsically too small to be accurately rendered by DFT, the fact that even HF gives better results is somewhat disturbing. Nevertheless, the observation that Hartree–Fock and HCTH/407 are somewhat capable of properly predicting the structure and energetics of the ammonia dimer system suggests that the problem at hand is not beyond the grasp of density functional methods as such.

IV. THE HCTH/407+ FUNCTIONAL: CONSTRUCTION AND PERFORMANCE

Considering that standard density functionals were shown to be unable to describe the energy difference between linear and bent hydrogen bonds and do not capture the large bending angle of the hydrogen bond, the most obvious remedy would be to change the functional form itself. However, if all tested functionals give such a bad description, this is unlikely to solve the problem. The culprit in this case, therefore, has to be the set of molecules which the HCTH functionals are fit to, insofar as only linearly hydrogen-bonded systems have been included. Nevertheless, including the minimum structure and energetics of the ammonia dimer determined in Sec. III into the set probably only partly solves

this problem. The main problem, as established before, is the energy difference between the linear and bent hydrogen bonds. In addition, the TZ2P basis set commonly used in the fit set might not be appropriate. Even when employing the A′PVTZ basis set mentioned earlier, the basis set superposition error for the dimerization energy is 29 cm^{-1}, contributing 8 cm^{-1} to the energy difference between the minimum and symmetric structure when using the B97-1 functional. In comparison, using the TZ2P basis set, the BSSE is 92 cm^{-1}, contributing 33 cm^{-1} to the energy difference. Clearly, the TZ2P basis set is inappropriate for this problem. The above-mentioned numbers indicate that a counterpoise procedure has to be employed within the fit in order to get a good estimate. Note that even when using an extrapolation to the full basis set limit (in the case of W2), the difference between the counterpoise corrected and uncorrected values is already 3 cm^{-1}.

All of the above-mentioned issues were considered in the fit. Thus, we fit to all points shown in Fig. 1 employing an A′PVTZ basis set with counterpoise correction in the fit. This is the first time we are fitting to nonequilibrium structures, and we only fit to their energy differences and exchange–correlation potentials of these. Due to the energy difference of only a couple of wave numbers, an additional weight has to be employed for any change in the fit to be noticeable. Thus, Eq. (3) now reads

$$\Omega = \sum_{m}^{n_E} w_m (E_m^{\text{exact}} - E_m^{\text{KS}} - E_m^{\text{BSSE}})^2 + \sum_{l,X}^{n_G} w_{l,G} \left(\frac{\partial E_l^{\text{KS}}}{\partial X} \right)^2$$

$$+ \sum_{j,\sigma}^{n_v} w_{j,v} \int (v_{j,\sigma}^{\text{ZMP}} + k_{j,\sigma} - v_{j,\sigma}^{\text{KS}})^2 \rho_{j,\sigma}^{2/3} d\mathbf{r} \qquad (5)$$

with

$$E_m^{\text{BSSE}} = E_m^{\text{ghost,donor}} + E_m^{\text{ghost,acceptor}}$$
$$- E_m^{\text{monomer,donor}} - E_m^{\text{monomer,acceptor}}. \qquad (6)$$

Since we do not want to fit to a given value of basis set superposition error, it is included in E_m^{KS}. The weights $w_{m,l,j}$ now also include the additional weights for the potential energy surface with the other weights defined as before.[82] Thus, w_m is composed of

$$w_{m,\text{PES}} = 750 \times \text{weight}_{\text{confidence}} \times \text{weight}_{\text{atom}}$$
$$\times \text{weight}_{\text{dimer}} \times \text{weight}_{\text{PES}}. \qquad (7)$$

When determining the weights for the new members of the fit set, we need to consider both their A′PVTZ optimized energies as well as their A′PVTZ single-point energies at the CCSD(T)/A′PVQZ optimized geometries. The latter is necessary since we can only fit to single points. As a result of the small energy differences, the frozen-geometry single-point energies and optimized energies differ by a significant amount. The development procedure is similar to the one employed for the HCTH/407 functional, and the set includes numerous atomization energies, proton affinities, ionization potentials, electron affinities, and dissociation energies of hydrogen-bonded dimers and transition metal complexes.[82] First, we fit to a subset of the 407 molecules in order to get

close to the global minimum, then we fit to the full set. The latter subset (small set) is the G2-1 set plus two hydrogen-bonded systems $(H_2O)_2$ and $(HF)_2$, and the additional structures on the potential energy surface, making 153 systems in all (the 147 of the HCTH/147 functional plus the five PES points, in addition to the NH_3 dissociation energy at the TZ2P basis). For each point on the PES, the counterpoise correction was employed. The results using the newly determined functionals as a function of the weights have been determined in both the first fit (to 153 systems) and the second fit (to 413 systems). Thus, we obtained new functionals with weights ranging from 0/0 (which corresponds to the HCTH/407 functional) to 200/200. The first weight is the one used in the subset, while the second corresponds to the large fit. The importance of the weights in the first fit can be seen from the differences by using weight pairs of 30/80 and 80/80—they differ by about a factor of 2 in the energy difference between the staggered and eclipsed geometry. Hence, the minimum obtained by the second fit will of necessity be close to the global minimum obtained by the first one. When increasing these weights, we approach the reference values as expected, with the 200/200 functional rendering the closest values to the reference method. While not explicitly included in the fit, the BSSE also increased from 0.444 to 0.866 kJ/mol. This resembles the tendency of the functional to have a larger intermolecular distance than the reference methods when increasing the weights, hence entering a regime where the BSSE increases more rapidly than for the optimized structures. In comparison, the largest BSSE observed by the functionals tested in Table III is 0.48 kJ/mol. However, for all the calculations in the fit we have performed only DFT single-point energy calculations at the CCSD(T) optimized geometries.

Another, more appropriate, point of comparison consists of the optimized structures of all the newly obtained functionals, as done in Table III for the contemporary functionals. Since the energy differences in general are very small, these results differ significantly from the ones obtained by the single-point energies calculated at the coupled-cluster geometries. In addition, the C_{2h} structure becomes the global minimum for the functionals with a weight of 80 or larger in the first fit. Based on these results, the 30/80 functional appears to be the most reliable for this interaction, and hence will be denoted as the new HCTH407+ functional. This new functional (compare to Table III) now renders a dissociation energy of 13.18 kJ/mol for the ammonia dimer, in much closer agreement to the reference values than any other method employed. The difference between the C_s minimum and the C_{2h} structure is 4.0 cm^{-1} for HCTH/407+, compared to our best estimate of 3.5 cm^{-1} in Table II. The staggered C_s structure lies 18 cm^{-1} above its eclipsed counterpart, which is about five wave numbers higher than our best estimate but still within its error bars. The difference to the linear eclipsed and linear staggered structures are slightly underestimated at 51.5 and 53.5 cm^{-1}, respectively, but this is still a vast improvement over the other functionals. In Fig. 2, we compare the energies of the new HCTH407+ functional to W2 and one of the most commonly used GGA functionals (BLYP). The BSSE for the relaxed C_s structures does
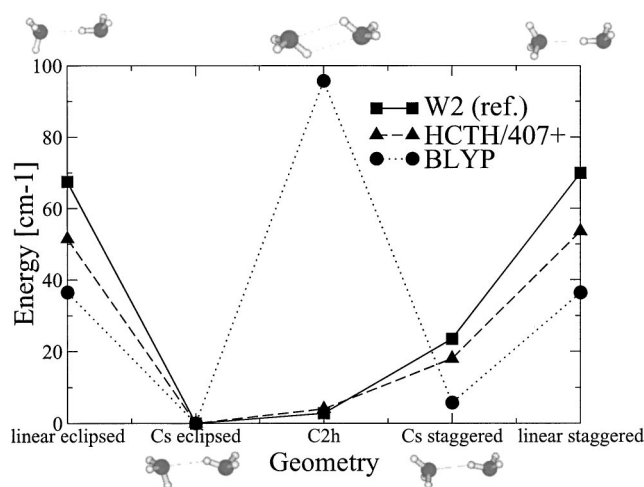

FIG. 2. The potential energy profile obtained from W2 theory (accurate reference calculations) in comparison to that obtained from HCTH407+ and BLYP functionals at the five optimized structures, see insets, from Fig. 1. Note that the profiles obtained from other GGA functionals such as PBE are qualitatively similar to that of BLYP.

not increase as rapidly as for their CCSD(T) optimized counterparts. It increases from 0.43 (HCTH/407) to 0.45 (HCTH/407+) to 0.61 kJ/mol (weight of 200), and does not yield as unreasonably large values as the single-point calculations at the CCSD(T) geometries. The hydrogen bond lengths of the C_s and C_{2h} structures increase with larger weights, emphasizing the importance of this analysis. Generally, all HCTH functionals are found to slightly overestimate this hydrogen bond length. The HNN angle of the HCTH407+ functional is 17° for the minimum geometry. This is within the accuracy that can be expected from contemporary density functionals ($\pm 2°$), showing a significant improvement over all other density functionals in Table IV. The results for all functionals obtained with different weights (from which we determined the HCTH407+ functional) are given in the supplementary material.[120]

The parameters which define the HCTH407+ functional, compared to HCTH/407, are given in Table V. As might be expected, they differ only slightly from those for the standard HCTH/407 functional; only the correlation and higher-order coefficients have significantly been affected by the change. Nevertheless, the new functional should now be able to describe nondirected hydrogen bonds better than HCTH/407. On the level of the ammonia dimer, the improvement with respect to other density functionals becomes clearly visible in Fig. 2; see Table III for the corresponding numbers. It is seen that HCTH407+ describes the relative stability of all isomers much better with respect to the W2 reference data than BLYP, which was selected as a prominent representative of the GGA family. Most important, the dramatic failure of BLYP to capture the stability of the cyclic C_{2h} isomer relative to all other isomers is cured. According to HCTH/407+, the two C_s structures as well as the C_{2h}

TABLE V. Expansion coefficients of the HCTH407+ functional compared to the coefficients of the HCTH/407 functional.

Functional	HCTH407+	HCTH/407
$c_1 = c_{X\sigma,0}$	1.080 18	1.081 84
$c_2 = c_{C\sigma\sigma,0}$	0.803 02	1.187 77
$c_3 = c_{C\alpha\beta,0}$	0.736 04	0.589 08
$c_4 = c_{X\sigma,1}$	−0.4117	−0.5183
$c_5 = c_{C\sigma\sigma,1}$	−1.0479	−2.4029
$c_6 = c_{C\alpha\beta,1}$	3.0270	4.4237
$c_7 = c_{X\sigma,2}$	2.4368	3.4256
$c_8 = c_{C\sigma\sigma,2}$	4.9807	5.6174
$c_9 = c_{C\alpha\beta,2}$	−10.075	−19.222
$c_{10} = c_{X\sigma,3}$	1.3890	−2.6290
$c_{11} = c_{C\sigma\sigma,3}$	−12.890	−9.1792
$c_{12} = c_{C\alpha\beta,3}$	20.611	42.572
$c_{13} = c_{X\sigma,4}$	−1.3529	2.2886
$c_{14} = c_{C\sigma\sigma,4}$	9.6446	6.2480
$c_{15} = c_{C\alpha\beta,4}$	−29.418	−42.005

structure are essentially degenerate, which is in accord with the reference data. Apart from the energetics, also the structure of the ground state of the ammonia dimer, i.e., the eclipsed C_s structure, is dramatically improved, see Table IV for details. In particular the hydrogen bond angle HNN is now much larger and thus closer to the reference value than *any* other density functional method; note that also the functionals PW91, B97-2, and PBE0 were considered. The same is true for the HNN angle in the staggered variant of the C_s symmetric structure. However, it is also clear from this table that the N···H distance is clearly overestimated: HCTH/407+ yields a distance of about 2.5 Å instead of around 2.3 Å as required. This seems to be typical for the HCTH family as both HCTH/120 and HCTH/407 yield similarly large values exceeding 2.4 Å (and HCTH/93 leads to 2.614 Å). In addition, the same trend of producing too long hydrogen bonds is found for the C_{2h} structure. This deficiency is corrected by both τ-HCTH and τ-HCTH hybrid functionals. Here it should be noted that both BLYP and PBE describe the hydrogen bond length quite well, however at the expense of making it much too linear and grossly disfavoring the cyclic structure energetically.

Furthermore, this significant improvement in describing nondirected hydrogen bonds, however, comes at the expense of a slightly increased error for the other molecules in the fit set. Table VI shows the errors of the HCTH/407 and HCTH407+ functionals to the fit set, summarizing these as rms energy and geometry errors, together with the errors for the energies, geometry shifts, and frequency shifts of nine hydrogen-bonded systems. The values for B3LYP, BLYP, and BP86 are included for comparison. The hydrogen-bonded systems are the $(HF)_2$, $(HCl)_2$, $(H_2O)_2$, $(CO)(HF)$, $(OC)(HF)$, $(FH)(NH_3)$, $(ClH)(NH_3)$, $(H_2O)(NH_3)$, and $(H_3O^+)(H_2O)$ complexes, but not the NH_3 dimer itself. The performance of other functionals over all the sets has been discussed elsewhere.[22,24,82] Overall, errors for the HCTH407+ functional are quite similar to HCTH/407, which in turn means that they are still excellent compared to first-generation hybrid functionals like B3LYP and especially GGA functionals like BLYP or BP86. Although we expect the geometries to be still slightly worse than B3LYP (although the gradient error is comparable), the energetic properties are better described, as are the hydrogen bonds. Whereas the errors of the HCTH407+ functional for the fit set have barely changed compared to HCTH/407, the accuracy of the dissociation energies of the nine directed hydrogen bonds has actually decreased by about 20%. Nonetheless, the accuracy of the frequency shifts of the H–X bond stretches has increased, indicating that we seem to have improved the description of the potential energy surface of these complexes.

V. LIQUID AMMONIA: STRUCTURE, DYNAMICS, AND HYDROGEN BONDING

A. Radial distribution functions

We have calculated the nitrogen–nitrogen, hydrogen–hydrogen, and nitrogen–hydrogen radial distribution functions (RDFs) from the atomic trajectories generated by *ab initio* molecular dynamics simulations; note again that we used the mass of the deuteron instead of that of the proton but we still use the symbol H for convenience. The results for both HCTH407+ and BLYP functionals are shown in Fig. 3. In this figure, we have also included the experimental results[66,121] of the RDFs of liquid ammonia at 273 K; note that the underlying experimental technique is based on the assumption that the structure of all isotopically substituted systems is identical. For the nitrogen–nitrogen RDF, it is seen that at the short distances the BLYP $g_{NN}(r)$ is in better agreement with experimental results. The HCTH407+ peak is located at a distance of about 0.15 Å larger than the experimental peak position whereas the BLYP peak appears at a somewhat shorter distance. We note in this context that the

TABLE VI. Comparison of the errors of the 407+ fit set for the HCTH407+ and previous published functionals. Also included are the errors for properties of nine hydrogen-bonded systems (see the text).

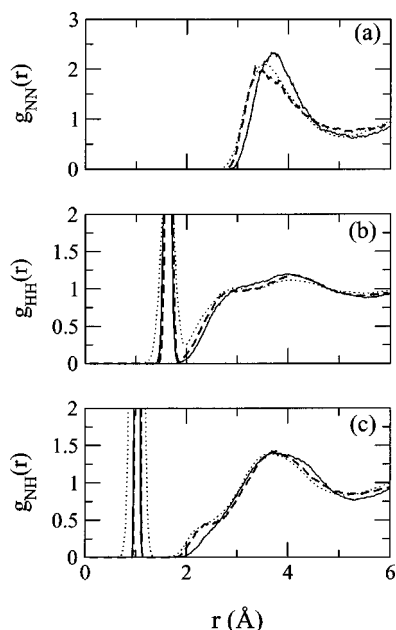| Property	407+ set of molecules		Hydrogen-bonded systems		
	rms energy (kcal/mol)	Σ gradient (a.u.)	rms dissociation energy(%)	rms H-bond shift (%)	rms frequency shift (%)
HCTH/120	9.1	11.51	8.5	26.0	29.1
HCTH/407	7.8	11.91	7.5	16.7	14.8
HCTH407+	8.0	11.96	10.3	16.8	12.8
B3LYP	9.4	12.00	11.0	30.2	35.0
BLYP	9.7	19.30	16.4	42.1	42.9
BP86	16.4	17.05	22.3	81.9	68.3

FIG. 3. The atom–atom radial distribution functions. The solid, dashed, and the dotted curves show the HCTH/407+, BLYP, and the experimental (Refs. 66 and 121) results, respectively.

HCTH407+ functional gives an overestimated equilibrium N–N distance for the isolated dimer compared to the reference CCSD(T) result as can be inferred from Table IV. The longer N–N distance seems to be translated to the liquid phase configurations and we observe a somewhat longer most probable N–N distance for the HCTH407+ functional than what is found in the experiments. Still, the overall shape of the first peak is represented reasonably well by both the functionals. When the RDFs are integrated up to their first minimum to obtain the coordination number in the first solvation shell, we obtained the values of 13.2 and 12.1 for HCTH407+ and BLYP functionals compared to an experimental value of 12.75. Clearly, the agreement with experimental results is found to be rather good.

Considering the results of the H–H and N–H RDFs, the positions of the calculated intramolecular H–H and N–H peaks for both the functionals agree rather well with experimental results, as expected. For example, the liquid phase N–H bond length and intramolecular H–H distance for the HCTH407+ (BLYP) functionals are 1.03 (1.03) Å and 1.63 (1.65) Å, which can be compared with the experimental values of 1.04 and 1.60 Å, respectively. Also, these intramolecular distances in the liquid phase are very close to their gas phase values. This was also noted earlier for the BLYP functional.[59] Because of the quantum disperson effects which are present in real liquid but not in the current simulated systems, the experimental intramolecular peaks are found to be broader than the theoretical peaks. The somewhat higher value of the experimental H–H correlation at the first minimum at around 2 Å can also be attributed to such quantum dispersion effects.

The intermolecular H–H peaks are found to be well represented by both functionals. The intermolecular part of the N–H RDF shows the presence of both H-bonded and non-

H-bonded H atoms in the first solvation shell. The shoulder up to about 2.7 Å can be attributed to hydrogen bonded H atoms, while the more pronounced peak at the larger distance at around 3.75 Å corresponds to the hydrogen atoms in the solvation shell which are not hydrogen bonded. Again, both functionals are found to describe well the non-hydrogen bonded first solvation shell peak when compared with the corresponding experimental result. For the hydrogen bonded part, however, the HCTH407+ result is found to exhibit a less pronounced shoulder than what is found in the experiments and for the BLYP functional. This is probably a result of the slight overestimation of the hydrogen bond length by HCTH407+ already on the level of the dimer, see Table IV. Considering both hydrogen bonded and non-hydrogen-bonded H atoms, a sphere of radius 5.3 (5.2) Å around a central N atom is found to contain 34.1 (34) intermolecular H atoms for the HCTH407+ (BLYP) functional. The radius of the sphere is set to 5.3 (5.2) Å because the first minimum of the intermolecular N–H RDF is located at this distance. The corresponding radius for the experimental N–H RDF is 5.0 Å, yielding the experimental value of 34.8 for the above-mentioned coordination number. A more detailed analysis of the distribution of hydrogen bonds in liquid ammonia is given in the Sec. V B, and the dynamical aspects of hydrogen bonds are considered in Sec. V D.

B. Distribution of hydrogen bonds

The analysis of the hydrogen bond (HB) distribution among ammonia molecules is based on a calculation of the fractions P_n of ammonia molecules that engage in n hydrogen bonds and the average number of hydrogen bonds that an ammonia molecule donates and accepts.[29] Following previous work on liquid ammonia, water and other hydrogen bonding liquids,[59,71,72,122–128] we have adopted a geometric definition of the hydrogen bonds where two ammonia molecules are assumed to be hydrogen bonded if they satisfy the following configurational criteria with respect to N–N and N–H distances:

$$R^{(NN)} < R_c^{(NN)},$$
$$R^{(NH)} < R_c^{(NH)}, \tag{8}$$

and the values of these distance cut-offs are usually determined from the positions of the first minimum of the corresponding (intermolecular) RDFs. We have used a similar procedure where the N–N RDF gives a value of $R_c^{NN} = 5.25$ (5.1) Å for the N–N cut-off for HCTH407+(BLYP) functionals. However, the procedure cannot be applied unambiguously to determine the N–H cut-off because no clear minimum that separates the hydrogen bonded and non-bonded H atoms is found in the N–H RDF. In the latter case, the shoulder which is assigned to hydrogen bonded H atoms merges into the broad and more intense peak corresponding to the H atoms of the first solvation shell which are not hydrogen bonded. Since this shoulder—which corresponds to the hydrogen bonded H atoms—extends up to about 2.7 Å in the experimental and BLYP RDFs we have taken this distance of 2.7 Å as the cutoff N–H distance. For HCTH/407 + also, we have used the same cut-off of the N–H distance
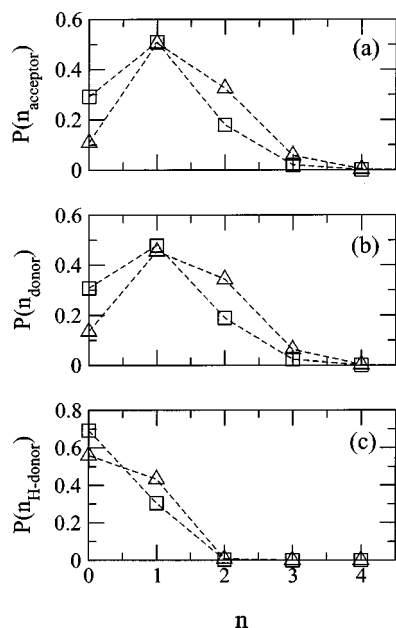
FIG. 4. The fraction $P(n)$ of molecules having a certain number of accepted $n_{acceptor}$ and donated n_{donor} hydrogen bonds, see panels (a) and (b), respectively. (c) The fraction of hydrogen atoms that donates a certain number of hydrogen bonds. The squares and the triangles represent the results for the HCTH407+ and BLYP functionals, respectively, and the dashed lines are drawn to guide the eye.

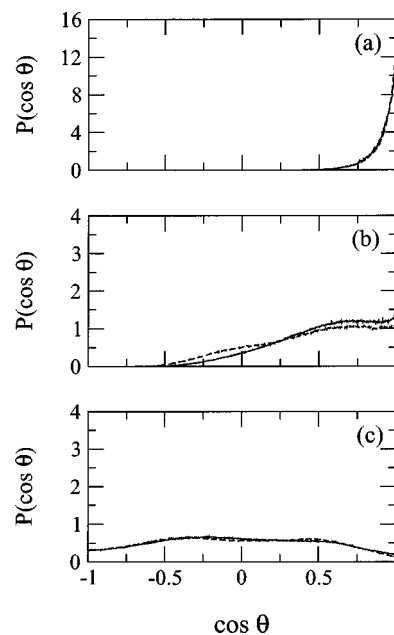FIG. 5. The distribution of the cosine of the N···N–H angle for H atoms that belong to the nearest neighbors. (a) The distribution for hydrogen bonded H atoms (i.e., $R^{(NH)} < 2.7$ Å). (b) and (c) The results for non-hydrogen-bonded H atoms that appear in the region 2.7 Å $< R^{(NH)} < 3.7$ Å and 3.7 Å $< R^{(NH)} < 4.7$ Å. The solid and the dashed curves show the results for the HCTH407+ and BLYP functionals, respectively.

although the hydrogen bonded shoulder is less pronounced for this functional. Still, variation of R_c^{NH} within reasonable bounds does not change qualitatively the result of this analysis.

In Fig. 4, we have shown the distribution of donor and acceptor hydrogen bonds for both HCTH407+ and BLYP functionals. Figures 4(a) and 4(b) show the fraction of ammonia molecules that accept or donate n hydrogen bonds and Fig. 4(c) shows the fraction of hydrogen atoms that donate n hydrogen bonds. The majority of the ammonia molecules is found to accept one hydrogen bond and to donate one. Also, the fraction of hydrogen atoms donating two or more hydrogen bonds is found to be negligibly small, which means that the bifurcated or multifurcated hydrogen bonds are practically absent in liquid ammonia. The average number of donor hydrogen bonds per ammonia molecule, which is also equal to the average number of acceptor hydrogen bonds per molecule, is found to be 0.93 (1.34) for the HCTH407+ (BLYP) functional. Given that there are as many as about 13 ammonia molecules in the first solvation shell, we conclude that non-hydrogen-bonded interactions, i.e., packing or steric effects, are crucial in determining the solvation behavior of ammonia in the liquid state. This is in sharp contrast to the case of liquid water where the solvation structure of a water molecule is determined primarily by hydrogen bonding interactions.[129]

The ammonia dimer has a strongly bent hydrogen bond in its equilibrium geometry and it would be interesting to investigate whether the hydrogen bonds remain bent in the liquid phase. We have carried out such an analysis by calculating the distribution function of the cosine of the hydrogen bond angle θ, which is defined as the N···N–H angle of a

hydrogen bonded pair and the results are shown in Fig. 5(a) for both the functionals. It is seen that, for both the functionals, the probability distribution $P(\cos\theta)$ is peaked at $\cos\theta = 1$ indicating that the *preferred hydrogen bond geometry is linear in the liquid phase*, see Ref. 130. The peak is somewhat more sharp and narrow for the BLYP functional, which indicates a stronger preference for the linear hydrogen bonds for this functional as compared to that for the HCTH407+ functional. This preferential presence of linear hydrogen bonds in the liquid phase is indeed an interesting result given that the dimer has a bent hydrogen bond in the gas phase. We have also investigated the distribution of N···N–H angle for H atoms that belong to nearest neighbors but are not hydrogen bonded, i.e., the N···H distance is greater than 2.7 Å. The results of these angular distributions are shown in Fig. 5(b) for 2.7 Å $< R^{(NH)} < 3.7$ Å and in Fig. 5(c) for 3.7 Å $< R^{(NH)} < 4.7$ Å. A wide range of values are found for the N···N–H angle with very little or no preference for a particular orientation. These findings are indeed consistent with the above-presented analysis that the first solvation shell in liquid ammonia is dominated by simple packing rather than by directional hydrogen bonding.

C. Self-diffusion and orientational relaxation

The translational self-diffusion coefficient of an ammonia molecule in the liquid state is calculated from the long-time limit of the mean-square displacement (MSD)

$$D = \lim_{t \to \infty} \frac{\langle [r(t) - r(0)]^2 \rangle}{6t}, \tag{9}$$

where $r(t)$ is the position of the center of mass of a molecule at time t and the average is carried out over the time origin for autocorrelation and over all the molecules as usual. The results of the diffusion coefficients, which are obtained from a least-squares linear fit of the simulation data excluding the initial ballistic regime up to 0.5 ps, are included in Table VII. This table also contains the experimental values of the diffusion coefficients of deuterated liquid ammonia ND_3 at 275 and 252 K that are found from Eq. (2) of Ref. 131, which was shown to fit the experimental data over a rather wide temperature range very well. The agreement of the calculated diffusion coefficients with the experimental result is found to be reasonably good for both functionals. In particular it is gratifying to see that the experimental value is *underestimated* because quantum effects on nuclear motion, which are neglected in the present study, tend to increase the diffusion in a liquid.

The self-orientational motion of ammonia molecules is analyzed by calculating the orientational time correlation function,[132] $C_l^\alpha(t)$, defined by

$$C_l^\alpha(t) = \frac{\langle P_l(e^\alpha(t) \cdot e^\alpha(0)) \rangle}{\langle P_l(e^\alpha(0) \cdot e^\alpha(0)) \rangle}, \qquad (10)$$

where P_l is the Legendre polynomial of order l and e^α is the unit vector which points along the α axis in the molecular frame. Here, we have studied the time dependence of $C_l^\alpha(t)$ for $l=1,2$ and for three different e^α, the unit vectors along the molecular dipole axis, a N–H bond, and an intramolecular H–H axis. The geometric dipole vector of an ammonia molecule is calculated by assigning partial charges to N and H atoms as given by the classical model of Ref. 71. For the orientational relaxation of unit vectors along the N–H and H–H axes, the results are averaged over three such intramolecular axes of each type. After an initial transient nonexponential decay, the relaxation becomes diffusional and $C_l^\alpha(t)$ decays exponentially. The orientational correlation time, τ_l^α, is defined as the time integral of the orientational correlation function

$$\tau_l^\alpha = \int_0^\infty dt\, C_l^\alpha(t). \qquad (11)$$

We note that the orientational relaxation of molecular vectors containing H atoms is usually measured by nuclear magnetic resonance (NMR) relaxation experiments, which yield the Fourier transform of a correlation function for $l=2$ such that the integrated correlation time τ_2^α is measured.

In Fig. 6, we depict the results of the orientational correlation function $C_l^\alpha(t)$ for $l=1,2$ and $\alpha=$dipole, N–H and H–H. The corresponding results of the orientational correlation times are included in Table VII. We have also included the experimental result of τ_2 of deuterated ammonia ND_3 as given by the fitted Arrhenius law of Ref. 133. Since this experimental relaxation time was obtained by NMR relaxation experiments, it is likely to correspond to the relaxation of N–H/H–H vectors rather than the dipole vector. The BLYP functional is found to predict a relatively slower orientational relaxation. Considering the quite small system size
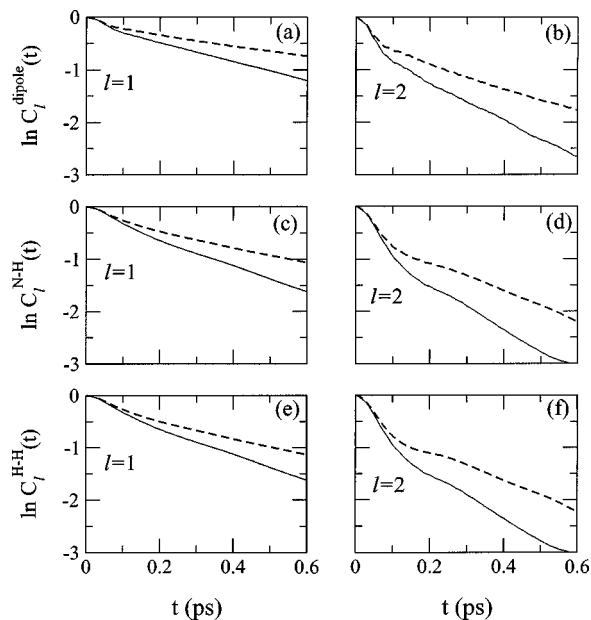

FIG. 6. The time dependence of various orientational correlation functions, see the text for definitions and further details. The solid and the dashed curves show the results for the HCTH407+ and BLYP functionals, respectively.

and short simulation trajectories, both functionals are found to describe the single-particle rotational dynamics of liquid ammonia reasonably well.

D. Dynamics of hydrogen bonds

The key dynamical quantity in the context of hydrogen bond dynamics is the mean hydrogen bond lifetime, τ_{HB}. The fast librational motion of ammonia molecules makes apparent breaking and reformation of a hydrogen bond a very fast process and, depending on how these fast transient events are taken into account, one can obtain different values for the hydrogen bond (HB) lifetime. The rotational motion of ammonia molecules is also a rather fast process and can also contribute to the short-time dynamics of hydrogen bonds. For a particular chosen definition of a breaking event, one can adopt a direct counting method[128,134,135] or a time correlation function method[123–127,136] to calculate the lifetime. In the present work, we have adopted the time correlation function approach which allows us to calculate the hydrogen bond lifetime in both cases: (a) The breaking of hydrogen bond occurs due to fast librational motion even though it may be a transient event and not a ''true'' breaking event and (b) these fast librational breaking events are ignored and only rotational and translational diffusional breaking on a longer time scale is considered as the ''true'' breaking of a hydrogen bond. Also, in the present context, it is implied that ''fast librational breaking'' also includes the effects of fast rotational motion that might contribute to the short-time dynamics of the hydrogen bonds.

In order to obtain the hydrogen bond lifetime for the two above-mentioned scenarios, we calculate three time correlation functions: one continuous and two intermittent hydrogen bond correlation functions.[123,124,136] Before we define these time correlations, we first define two hydrogen bond popula-

J. Chem. Phys., Vol. 119, No. 12, 22 September 2003
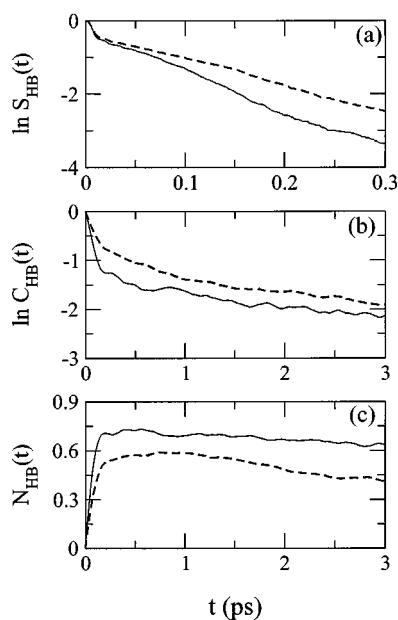
Hydrogen bonding in ammonia 5977

FIG. 7. The time dependence of various hydrogen bond correlation functions, see the text for definitions and further details. The different curves are labeled as in Fig. 6.

TABLE VII. Dynamical properties of liquid ammonia. The diffusion coefficient, relaxation times, and the inverse rate constants are expressed in units of 10^{-5} cm^2 s^{-1}, ps, and ps, respectively. Note that *all* numbers given refer to the fully deuterated species ND$_3$.

Quantity	HCTH407+	BLYP	Experiment
D	5.23	5.44	8.75,[a] 5.95[b]
τ_1^{dipole}	0.52	0.85	
τ_1^{NH}	0.37	0.58	
τ_1^{HH}	0.34	0.54	
τ_2^{dipole}	0.18	0.27	
τ_2^{NH}	0.15	0.22	
τ_2^{HH}	0.15	0.22	
τ_2^{exp}			0.26,[a] 0.35[b]
τ_{HB}	0.07	0.10	
$1/k_{short}$	0.10	0.16	
$1/k_{long}$	0.62	0.60	

[a]At 275 K.
[b]At 252 K.

tion variables $h(t)$ and $H(t)$: $h(t)$ is unity when a particular tagged pair of ammonia molecules is hydrogen bonded at time t, according to the adopted definition from Sec. V B and zero otherwise. The function $H(t)$ is unity if the tagged pair of ammonia molecules remains continuously hydrogen bonded from $t=0$ to time t given that the bond was formed for the last time at $t=0$, and it is zero otherwise. We define the continuous hydrogen bond time correlation function $S_{HB}(t)$ as

$$S_{HB}(t)=\langle h(0)H(t)\rangle/\langle h\rangle, \qquad (12)$$

where $\langle\cdots\rangle$ denotes an average over all hydrogen bonds that are created at $t=0$. Clearly, $S_{HB}(t)$ describes the probability that a hydrogen bonded ammonia pair, which was created at $t=0$, remains continuously bonded up to time t. It differs from the continuous hydrogen bond correlation function of Rapaport[136] in that we apply the condition of bond formation at time $t=0$. The mean hydrogen bond lifetime τ_{HB} can then be calculated from the time integral

$$\tau_{HB}=\int_0^\infty S_{HB}(t)dt. \qquad (13)$$

In Fig. 7(a), we have shown the decay of $S_{HB}(t)$ for both functionals and the corresponding results of τ_{HB} are included in Table VII. The hydrogen bond lifetime is found to be about 0.1 ps for both functionals. We note that both fast librational and slower diffusional motion can contribute to the decay of $S_{HB}(t)$. Since the librational motion occurs on a faster time scale and since the correlation function $S_{HB}(t)$ does not allow any reformation event, the dynamics of $S_{HB}(t)$ primarily reveal the dynamics of hydrogen bond breaking due to fast librational motion and hence the lifetime that is obtained from Eq. (12) corresponds to the average time over which a hydrogen bond survives before it "breaks" due to librations. Again, this short time breaking

may also include contributions from fast rotational motion of ammonia molecules which also occurs at subpicosecond time scale.

A different way to analyze the hydrogen bond dynamics is to calculate the intermittent hydrogen bond correlation function[123,136]

$$C_{HB}(t)=\langle h(0)h(t)\rangle/\langle h\rangle, \qquad (14)$$

where the average is now over all hydrogen bonds that were present at $t=0$. Note that the correlation function $C_{HB}(t)$ does not depend on the continuous presence of a hydrogen bond. It describes the probability that a hydrogen bond is intact at time t, given it was intact at time zero, independent of possible breaking in the interim time. Clearly, bonds which were briefly "broken" by fast librational motions would continue to contribute to the correlation function at later times and this leads to a much slower decay of $C_{HB}(t)$ at longer times. The results of $C_{HB}(t)$ are shown in Fig. 7(b), which clearly shows a two-phase relaxation of this correlation function. The initial fast relaxation corresponds to rapid breaking of hydrogen bonds due to librational motion and the slower relaxation after this initial transient decay corresponds to the breaking and reformation of hydrogen bonds due to both rotational and translational diffusion of ammonia molecules.

After a hydrogen bond is broken, the two ammonia molecules can remain in the vicinity of each other for some time before either the bond is reformed or the molecules diffuse away from each other. We define $N_{HB}(t)$ as the time-dependent probability that a hydrogen bond is broken at time zero but the two molecules remain in the vicinity of each other, i.e., as nearest neighbors but not hydrogen bonded at time t. Following previous work,[123] we can then write a simple rate equation for the "reactive flux" $-dC_{HB}/dt$ in terms of $C_{HB}(t)$ and $N_{HB}(t)$,

$$-\frac{dC_{HB}(t)}{dt}=kC_{HB}(t)-k'N_{HB}(t), \qquad (15)$$

where k and k' are the forward and backward rate constants for hydrogen bond breaking. The inverse of k can be interpreted as the average lifetime of a hydrogen bond.

The derivative of the intermittent hydrogen bond correlation or the "reactive flux" of Eq. (14) is computed from the simulation results of $C_{HB}(t)$ that are presented in Fig. 7(b). The probability function $N_{HB}(t)$ is also calculated from the simulation trajectories through the following correlation function approach:[124]

$$N_{HB}(t) = \langle h(0)[1 - h(t)]h'(t)\rangle / \langle h \rangle, \tag{16}$$

where $h'(t)$ is unity if the N–N distance of the pair of ammonia molecules is less than $R_c^{(NN)}$ at time t and it is zero otherwise. The results of $N_{HB}(t)$ are shown in Fig. 7(c). We used a least-squares fit of Eq. (14) to the simulation results of the reactive flux, $C_{HB}(t)$ and $N_{HB}(t)$ to produce the forward and backward rate constants. We performed the fitting in the short time region $0 < t < 0.15$ ps to obtain the rate constants and the corresponding average hydrogen bond lifetime for the librational relaxation and we also carried out the fitting on the longer time region 0.25 ps $< t < 3$ ps to calculate these quantities for slower rotational and translational diffusional relaxation. The inverses of the corresponding forward rate constants, which correspond to the average hydrogen bond lifetimes and which we denote as $1/k_{short}$ and $1/k_{long}$, are included in Table VII. We note that the value of $1/k_{short}$ is very close to average hydrogen bond lifetime τ_{HB} obtained from the continuous hydrogen bond correlation function $S_{HB}(t)$ which is not unexpected because both $S_{HB}(t)$ and the short-time part of the "reactive flux" capture the hydrogen bond "breaking" dynamics due to fast librational motion. The hydrogen bond lifetime as given by $1/k_{long}$ is significantly longer because it excludes the fast librational relaxation.

VI. SUMMARY AND CONCLUSIONS

We have investigated the properties of ammonia from the gas phase dimer to the liquid state by means of wave-function-based quantum chemistry techniques, density functional theory, and *ab initio* molecular dynamics. The ammonia dimer is a particularly interesting hydrogen-bonded system, as it is known to feature a strongly bent hydrogen bond. In order to investigate possible consequences of this nonlinear hydrogen bond, important points on the potential energy surface were first investigated by means of *ab initio* methods up to W2-extrapolated CCSD(T) theory, see Fig. 1 for the corresponding structures. The structure and energetics of important isomers are obtained up to unprecedented accuracy without resorting to experiment; see Fig. 1 and Table IV for structures, and Fig. 2 and Table III for energies. It is confirmed that the structure of the global minimum (having eclipsed C_s symmetry) possesses a substantially nonlinear hydrogen bond with an H–N···N angle that is predicted to be 20.7°; note that the corresponding angle is predicted to be 5.5° in the water dimer. The energy difference between the global minimum and the C_{2h} transition state (which is the famous "cyclic structure") is about 3.5 cm^{-1}, and the energy penalty to make the hydrogen bond artificially linear

amounts to only 70 cm^{-1}, i.e., 0.2 kcal/mol or 0.009 eV. This implies that the potential energy surface is *very* flat.

However, when investigating the ammonia dimer using a wide variety of available density functionals (including important representatives of the GGA, meta-GGA, and hybrid functional families) it was found that *none* of the functionals checked by us describes the bent hydrogen bond in $(NH_3)_2$ satisfactorily. Typically, the hydrogen bond angle is too small by a factor of 2 and the energy of the cyclic C_{2h} structure with respect to the eclipsed C_s global minimum is overestimated by a factor of 10 to 30. Since ammonia is an important hydrogen bonded liquid, a density functional was developed for studying this subtle system, with particular focus on its applicability for condensed phase simulations in the framework of Car–Parrinello molecular dynamics. To this end, a novel GGA-type density functional, HCTH/407+, was developed, with special emphasis on the nonlinear hydrogen bond and potential energy surface of $(NH_3)_2$. This functional yields the bent hydrogen-bonded equilibrium structure of the ammonia dimer, as well as the correct energetics of the low-lying isomers including the energy barrier to a linear hydrogen bond.

The performance of the new functional in describing the structural and dynamical properties of liquid ammonia was investigated by carrying out Car–Parrinello molecular dynamics simulations of the liquid phase. In addition, simulations were carried out using a GGA-type functional that is widely used for describing associated liquids, BLYP, and the results of the two functionals are compared with experiments wherever available. In particular, we focused on the atom–atom radial distribution functions, on structure and dynamics of hydrogen bonds, and on diffusion as well as orientational relaxation processes. Overall, both functionals are found to describe the structural and dynamical properties of the liquid phase reasonably well. Importantly, it is shown that the propensity to form a strongly bent hydrogen bond—which is characteristic for the equilibrium structure of the gas-phase ammonia dimer—is overwhelmed by steric packing effects that clearly dominate the solvation shell structure in the liquid state. Similarly, the propensity of ammonia molecules to form bifurcated and multifurcated hydrogen bonds in the liquid phase is found to be negligibly small. Thus, even functionals that lead to unreasonably linear hydrogen bonds in the limiting case of the *in vacuo* ammonia dimer, such as BLYP, yield a good description of *liquid* ammonia—albeit for the wrong reason!

J. Chem. Phys., Vol. 119, No. 12, 22 September 2003

Hydrogen bonding in ammonia   5979

[1] W. Kohn, Rev. Mod. Phys. **71**, 1253 (1999); J. A. Pople, Angew. Chem., Int. Ed. Engl. **38**, 1894 (1999); Angew. Chem. **111**, 2014 (1999).

[2] A. K. Rappé and E. R. Bernstein, J. Phys. Chem. A **104**, 6117 (2000).

[3] T. van Mourik and R. J. Gdanitz, J. Chem. Phys. **116**, 9620 (2002).

[4] M. Kamiya, T. Tsuneda, and K. Hirao, J. Chem. Phys. **117**, 6010 (2002).

[5] K. Laasonen, F. Csajka, and M. Parrinello, Chem. Phys. Lett. **194**, 172 (1992).

[6] F. Sim, A. St-Amant, I. Papai, and D. R. Salahub, J. Am. Chem. Soc. **114**, 4391 (1992).

[7] K. Laasonen, M. Sprik, M. Parrinello, and R. Car, J. Chem. Phys. **99**, 9080 (1993).

[8] K. Laasonen, M. Parrinello, R. Car, C. Lee, and D. Vanderbilt, Chem. Phys. Lett. **207**, 208 (1993).

[9] M. E. Tuckerman, K. Laasonen, M. Sprik, and M. Parrinello, J. Phys. Chem. **99**, 5749 (1995); J. Chem. Phys. **103**, 150 (1995).

[10] M. Sprik, J. Hutter, and M. Parrinello, J. Chem. Phys. **105**, 1142 (1995).

[11] P. L. Silvestrelli and M. Parrinello, Phys. Rev. Lett. **82**, 3308 (1999); J. Chem. Phys. **111**, 3572 (1999).

[12] P. L. Silvestrelli, M. Bernasconi, and M. Parrinello, Chem. Phys. Lett. **277**, 478 (1997).

[13] D. Marx, M. E. Tuckerman, J. Hutter, and M. Parrinello, Nature (London) **397**, 601 (1999).

[14] M. Boero, K. Terakura, T. Ikeshoji, C. C. Liew, and M. Parrinello, Phys. Rev. Lett. **85**, 3245 (2000); J. Chem. Phys. **115**, 2219 (2001).

[15] E. Schwegler, G. Galli, and F. Gygi, Phys. Rev. Lett. **84**, 2429 (2000).

[16] E. Schwegler, G. Galli, F. Gygi, and R. Q. Hood, Phys. Rev. Lett. **87**, 265501 (2001).

[17] A. D. Boese, N. L. Doltsinis, N. C. Handy, and M. Sprik, J. Chem. Phys. **112**, 1670 (2000).

[18] M. E. Tuckerman, D. Marx, and M. Parrinello, Nature (London) **417**, 925 (2002).

[19] M. Krack, A. Gambirasio, and M. Parrinello, J. Chem. Phys. **117**, 9409 (2002).

[20] S. Izvekov and G. A. Voth, J. Chem. Phys. **116**, 10372 (2002).

[21] B. Paizs and S. Suhai, J. Comput. Chem. **19**, 575 (1998).

[22] C. Tuma, A. D. Boese, and N. C. Handy, Phys. Chem. Chem. Phys. **1**, 3939 (1999), note that the HCTH/120 functional is denoted HCTH-38 in this paper.

[23] K. N. Rankin and R. J. Boyd, J. Comput. Chem. **22**, 1590 (2001).

[24] A. D. Boese and N. C. Handy, J. Chem. Phys. **116**, 9559 (2002).

[25] D. D. Nelson, Jr., G. T. Fraser, and W. Klemperer, Science **238**, 1670 (1987).

[26] M. Havenith, *Infrared Spectroscopy of Molecular Clusters* (Springer, Verlag, Berlin, 2002), see in particular Chap. 9.

[27] W. Klopper, J. G. C. M. van Duijneveldt-van de Rijdt, and F. B. van Duijneveldt, Phys. Chem. Chem. Phys. **2**, 2227 (2000); see in particular the last line of Table 1.

[28] T. Steiner, Angew. Chem., Int. Ed. Engl. **41**, 48 (2002), Angew. Chem. **114**, 50 (2002).

[29] Note that we adopt here Steiner's terminology (Ref. 28): (i) in a hydrogen bond $\mathcal{D}$-H$\cdots\mathcal{A}$ the group $\mathcal{D}$-H is called the (proton) donor and $\mathcal{A}$ is called the (proton) acceptor; (ii) the interaction of one donor with two or more acceptors $\mathcal{A}', \mathcal{A}'', \ldots$ leads to so-called bifurcated $\mathcal{D}$-H$\overset{\mathcal{A}'}{\underset{\mathcal{A}''}{\cdots}}$ or multifurcated hydrogen bonds. Note that sometime the cyclic C_{2h} structure of $(NH_3)_2$ according to Fig. 1(e) is also termed "bifurcated," which we do not do here.

[30] R. Preißner, U. Egner, and W. Saenger, FEBS Lett. **288**, 192 (1991).

[31] Z. Latajka and S. Scheiner, J. Chem. Phys. **81**, 407 (1984).

[32] M. J. Frisch, J. E. Del Bene, J. S. Binkley, and H. F. Schaefer III, J. Chem. Phys. **84**, 2279 (1986).

[33] S. Liu, C. E. Dykstra, K. Kolenbrander, and J. M. Lisy, J. Chem. Phys. **85**, 2077 (1986).

[34] K. Hirao, T. Fujikawa, H. Konishi, and S. Yamabe, Chem. Phys. Lett. **104**, 184 (1984).

[35] K. P. Sagarik, R. Ahlrichs, and S. Brode, Mol. Phys. **57**, 1247 (1986).

[36] Z. Latajka and S. Scheiner, J. Chem. Phys. **84**, 341 (1986).

[37] D. D. Nelson, Jr., G. T. Fraser, and W. Klemperer, J. Chem. Phys. **83**, 6201 (1985).

[38] F.-M. Tao and W. Klemperer, J. Chem. Phys. **99**, 5976 (1993).

[39] D. M. Hassett, C. J. Marsden, and B. J. Smith, Chem. Phys. Lett. **183**, 449 (1991).

[40] M. Havenith, R. C. Cohen, K. L. Busarow, D. H. Gwo, Y. T. Lee, and R. J. Saykally, J. Chem. Phys. **94**, 4776 (1991).

[41] M. Havenith, H. Linnartz, E. Zwart, A. Kips, J. J. ter Meulen, and W. L. Meerts, Chem. Phys. Lett. **193**, 261 (1992).

[42] J. G. Loeser, C. A. Schmuttenmaer, R. C. Cohen, M. J. Elrod, D. W. Steyert, R. J. Saykally, R. E. Bumgarner, and G. A. Blake, J. Chem. Phys. **97**, 4727 (1992).

[43] R. J. Saykally and G. A. Blake, Science **259**, 1570 (1993).

[44] H. Linnartz, A. Kips, W. L. Meerts, and M. Havenith, J. Chem. Phys. **99**, 2449 (1993).

[45] N. Heineking, W. Stahl, E. H. T. Olthof, P. E. S. Wormer, and M. Havenith, J. Chem. Phys. **102**, 8693 (1995).

[46] H. Linnartz, W. L. Meerts, and M. Havenith, Chem. Phys. **193**, 327 (1995).

[47] G. Cotti, H. Linnartz, W. L. Meerts, A. van der Avoird, and E. H. T. Olthof, J. Chem. Phys. **104**, 3898 (1996).

[48] E. H. T. Olthof, A. van der Avoird, and P. E. S. Wormer, J. Chem. Phys. **101**, 8430 (1994).

[49] E. H. T. Olthof, A. van der Avoird, P. E. S. Wormer, J. G. Loeser, and R. J. Saykally, J. Chem. Phys. **101**, 8443 (1994).

[50] Note that the results for the 18-dimensional equilibrium structure of the ammonia dimer reported in Ref. 48 were obtained by (i) keeping the structure of the NH_3 monomers rigid, (ii) solving the remaining six-dimensional vibration–rotation–tunneling problem on a global potential energy surface, and (iii) adjusting some parameters of this *ab initio*-based potential in order to match the observed far-infrared spectrum (Ref. 42). Note that recent work on the water dimer (Ref. 51) showed that monomer flexibility does play a significant role in determining the vibration–rotation–tunneling spectrum of this dimer. The intramolecular degrees of freedom of the monomers are also expected to play a role in determining the "experimental" structure of the ammonia dimer.

[51] C. Leforestier, F. Gatti, R. S. Fellers, and R. J. Saykally, J. Chem. Phys. **117**, 8710 (2002).

[52] M. Behrens, U. Buck, R. Fröchtenicht, M. Hartmann, and M. Havenith, J. Chem. Phys. **107**, 7179 (1997).

[53] J. S. Lee and S. Y. Park, J. Chem. Phys. **112**, 230 (2000).

[54] J. Stalring, M. Schütz, R. Lindh, G. Karlström, and P.-O. Widmark, Mol. Phys. **100**, 3389 (2002).

[55] W. Klopper and H. P. Lüthi, Mol. Phys. **96**, 559 (1999).

[56] T. H. Zhu and W. T. Yang, Int. J. Quantum Chem. **49**, 613 (1994).

[57] M. Kieninger and S. Suhai, J. Comput. Chem. **17**, 1508 (1996).

[58] B. S. Jursic, J. Mol. Struct.: THEOCHEM **434**, 29 (1998).

[59] M. Diraison, G. J. Martyna, and M. E. Tuckerman, J. Chem. Phys. **111**, 1096 (1999).

[60] I. Olovsson and D. H. Templeton, Acta Crystallogr. **12**, 832 (1959).

[61] R. Boese, N. Niederprüm, D. Bläser, A. Maulitz, M. Y. Antipin, and P. R. Mallinson, J. Phys. Chem. B **101**, 5794 (1997).

[62] J. S. Loveday, R. J. Nelmes, W. G. Marshall, J. M. Besson, S. Klotz, and G. Hamel, Phys. Rev. Lett. **76**, 74 (1996).

[63] A. D. Fortes, J. P. Brodholt, I. G. Wood, and L. Vocadlo, J. Chem. Phys. **118**, 5987 (2003).

[64] A. H. Narten, J. Chem. Phys. **49**, 1692 (1968); **66**, 3117 (1977).

[65] P. Chieux and H. Bertagnolli, J. Phys. Chem. **88**, 3726 (1984).

[66] M. A. Ricci, M. Nardone, F. P. Ricci, C. Andreani, and A. K. Soper, J. Chem. Phys. **102**, 7650 (1995).

[67] W. L. Jorgensen and M. Ibrahim, J. Am. Chem. Soc. **102**, 3309 (1979).

[68] R. H. Kincald and H. A. Scheraga, J. Phys. Chem. **86**, 833 (1982).

[69] R. W. Impey and M. L. Klein, Chem. Phys. Lett. **104**, 579 (1984).

[70] S. V. Hannongbua, T. Ishida, E. Spohr, and K. Heinzinger, Z. Naturforsch., A: Phys. Sci. **43**, 572 (1988).

[71] J. Gao, X. Xia, and T. F. George, J. Phys. Chem. **97**, 9241 (1993).

[72] M. Kiselev, T. Kerdcharoen, S. Hannongbua, and K. Heinzinger, Chem. Phys. Lett. **327**, 425 (2000).

[73] T. A. Beu and U. Buck, J. Chem. Phys. **114**, 7848 (2001); see also **114**, 7853 (2001).

[74] S. Hannongbua, J. Chem. Phys. **113**, 4707 (2000).

[75] R. Car and M. Parrinello, Phys. Rev. Lett. **55**, 2471 (1985).

[76] D. Marx and J. Hutter, in *Modern Methods and Algorithms of Quantum Chemistry*, edited by J. Grotendorst (NIC, FZ Jülich, 2000); for down-

loads see www.theochem.ruhr-uni-bochum.de/go/cprev.html

[77] Y. Liu and M. E. Tuckerman, J. Phys. Chem. B **105**, 6598 (2001).

[78] R. N. Barnett and U. Landman, Phys. Rev. B **48**, 2081 (1993).

[79] A. D. Becke, J. Chem. Phys. **98**, 5648 (1993).

[80] F. A. Hamprecht, A. J. Cohen, D. J. Tozer, and N. C. Handy, J. Chem. Phys. **109**, 6264 (1998).

[81] A. D. Becke, J. Chem. Phys. **107**, 8554 (1997).

[82] A. D. Boese and N. C. Handy, J. Chem. Phys. **114**, 5497 (2001).

[83] D. C. Langreth and J. P. Perdew, Phys. Rev. B **21**, 5469 (1980).

[84] M. Levy and J. P. Perdew, Phys. Rev. A **32**, 2010 (1985).

[85] E. H. Lieb and S. Oxford, Int. J. Quantum Chem. **19**, 427 (1981).

[86] G. K.-L. Chan and N. C. Handy, Phys. Rev. A **59**, 3075 (1999).

[87] J. P. Perdew and K. Burke, Int. J. Quantum Chem. **57**, 309 (1996).

[88] Q. Zhao, R. C. Morrison, and R. G. Parr, Phys. Rev. A **50**, 2138 (1994).

[89] G. Menconi, P. J. Wilson, and D. J. Tozer, J. Chem. Phys. **114**, 3958 (2001).

[90] http://www-theor.ch.cam.ac.uk/people/nch/fit/; see also supplementary material to Ref. 82, EPAPS Document No. E-JCPSA6-301111.

[91] L. A. Curtiss, K. Raghavachari, P. C. Redfern, and J. A. Pople, J. Chem. Phys. **112**, 7374 (2000).

[92] J. M. L. Martin and G. De Oliveira, J. Chem. Phys. **111**, 1843 (1999).

[93] R. A. Kendall, T. H. Dunning, and R. J. Harrison, J. Chem. Phys. **96**, 6796 (1992).

[94] MOLPRO is a package of *ab initio* programs written by H.-J. Werner and P. J. Knowles, with contributions from J. Almlöf, R. D. Amos, A. Berning *et al.*

[95] L. A. Curtiss, K. Raghavachari, G. W. Trucks, and J. A. Pople, J. Chem. Phys. **94**, 7221 (1991).

[96] S. Parthiban and J. M. L. Martin, J. Chem. Phys. **114**, 6014 (2001).

[97] M. B. Sullivan, M. A. Iron, P. C. Redfern, J. M. L. Martin, L. A. Curtiss, and L. Radom, J. Phys. Chem. A (to be published).

[98] J. Noga and R. J. Bartlett, J. Chem. Phys. **86**, 7041 (1987), erratum **89**, 3401 (1988).

[99] J. F. Stanton, J. Gauss, J. D. Watts, W. Lauderdale, and R. J. Bartlett (1996) ACES II, an *ab initio* program system, incorporating the MOLECULE vectorized molecular integral program by J. Almlöf and P. R. Taylor, and a modified version of the ABACUS integral derivative package by T. Helgaker, H. J. Aa. Jensen, P. Jørgensen, J. Olsen, and P. R. Taylor.

[100] S. A. Kucharski and R. J. Bartlett, Chem. Phys. Lett. **158**, 550 (1989); K. Raghavachari, J. A. Pople, E. S. Replogle, and M. Head-Gordon, J. Phys. Chem. **94**, 5579 (1990).

[101] R. A. Chiles and C. E. Dykstra, J. Chem. Phys. **74**, 4544 (1981).

[102] N. C. Handy, J. A. Pople, M. Head-Gordon, K. Raghavachari, and G. W. Trucks, Chem. Phys. Lett. **164**, 185 (1989).

[103] M. J. Frisch *et al.*, GAUSSIAN 98, Revision A.11, Gaussian, Inc., Pittsburgh, PA, 1998.

[104] The Cambridge Analytic Derivatives Package (Cadpac), Issue 6.5, Cambridge (1998). Developed by R. D. Amos with contributions from I. L. Alberts, J. S. Andrews, S. M. Colwell *et al.*,

[105] A. D. Becke, Phys. Rev. A **38**, 3098 (1988); C. Lee, W. Yang, and R. G. Parr, Phys. Rev. B **37**, 785 (1988).

[106] J. P. Perdew, K. Burke, and M. Ernzerhof, Phys. Rev. Lett. **77**, 3865 (1996).

[107] J. P. Perdew, Phys. Rev. B **33**, 8822 (1986).

[108] J. P. Perdew and Y. Wang, Phys. Rev. B **45**, 13244 (1992), J. P. Perdew, J. A. Chevary, S. H. Vosko, K. A. Jackson, M. R. Pederson, D. J. Singh, and C. Fiolhais, *ibid.* **46**, 6671 (1992).

[109] P. J. Wilson, T. J. Bradley, and D. J. Tozer, J. Chem. Phys. **115**, 9233 (2001).

[110] C. Adamo and V. Barone, Chem. Phys. Lett. **298**, 113 (1998).

[111] S. F. Boys and F. Bernardi, Mol. Phys. **19**, 553 (1970).

[112] T. H. Dunning, J. Chem. Phys. **55**, 716 (1971).

[113] CPMD Program, J. Hutter, A. Alavi, T. Deutsch, M. Bernasconi, St. Goedecker, D. Marx, M. Tuckerman, and M. Parrinello, MPI für Festkörperforschung and IBM Zurich Research Laboratory.

[114] W. Kohn and L. J. Sham, Phys. Rev. A **140**, 1133 (1965).

[115] S. Goedecker, M. Teter, and J. Hutter, Phys. Rev. B **54**, 1703 (1996).

[116] E. Tsuchida, Y. Kanada, and M. Tsukada, Chem. Phys. Lett. **311**, 236 (1999).

[117] W. Klopper, M. Quack, and A. Suhm, J. Chem. Phys. **108**, 10096 (1998).

[118] C. J. Wormald and B. Wurzberger, J. Chem. Thermodyn. **33**, 1193 (2001).

[119] J. M. L. Martin, Chem. Phys. Lett. **242**, 343 (1995).

[120] See EPAPS Document No. E-JCPSA6-119-305335 for Tables I–III for different weights in order to determine the HCTH407+ functional to give the correct description of bonding in the ammonia dimer. A direct link to this document may be found in the online article's HTML reference section. The document may also be reached via the EPAPS homepage (http://www.aip.org/pubservs/epaps.html) or from ftp.aip.org in the directory /epaps/. See the EPAPS homepage for more information.

[121] The experimental RDFs that are plotted in Fig. 3 were derived from the diffraction data of Ref. 66 but using a more sophisticated procedure; A. K. Soper (private communication).

[122] A. Geiger, F. H. Stillinger, and A. Rahman, J. Chem. Phys. **70**, 4185 (1979).

[123] A. Luzar and D. Chandler, Phys. Rev. Lett. **76**, 928 (1996); Nature (London) **379**, 53 (1996); A. Luzar, J. Chem. Phys. **113**, 10663 (2000).

[124] H. Xu and B. J. Berne, J. Phys. Chem. B **105**, 11929 (2001); H. Xu, H. A. Stern, and B. Berne, *ibid.* **106**, 2054 (2002).

[125] F. W. Starr, J. K. Nielsen, and H. E. Stanley, Phys. Rev. Lett. **82**, 2294 (1999); Phys. Rev. E **62**, 579 (2000).

[126] A. Chandra, Phys. Rev. Lett. **85**, 768 (2000).

[127] S. Balasubramanian, S. Pal, and B. Bagchi, Phys. Rev. Lett. **89**, 115505 (2002).

[128] M. Ferrario, M. Haughney, I. R. McDonald, and M. L. Klein, J. Chem. Phys. **93**, 5156 (1990).

[129] F. H. Stillinger, Adv. Chem. Phys. **31**, 1 (1975); Science **209**, 451 (1980).

[130] J. Kroon and J. A. Kanters, Nature (London) **248**, 667 (1974).

[131] D. E. O'Reilly, E. M. Peterson, and C. E. Scheie, J. Chem. Phys. **58**, 4072 (1973).

[132] R. W. Impey, P. A. Madden, and I. R. McDonald, Mol. Phys. **46**, 513 (1982); see in particular Sec. 5.

[133] E. H. Hardy, A. Zygar, M. D. Zeidler, M. Holz, and F. D. Sacher, J. Chem. Phys. **114**, 3174 (2001).

[134] M. Haughney, M. Ferrario, and I. R. McDonald, J. Phys. Chem. **91**, 4934 (1987).

[135] R. D. Mountain, J. Chem. Phys. **103**, 3084 (1995).

[136] D. C. Rapaport, Mol. Phys. **50**, 1151 (1983).